EE

MAX-PLANCK-INSTITUT FÜR PHYSIK

WERNER-HEISENBERG-INSTITUT

MPI PhE 93.33
SCU 9417

MPI-PhE/93-33

December 1993

CERN LIBRARIES, GENEVA
P00022772

X-ray Polarimetry using the Photoeffect in a CCD-Detector

G. Buschhorn, R. Kotthaus, W. Kufner, W. Rößl, M. Rzepka, K.H. Schmidt

Max-Planck-Institut für Physik (Werner-Heisenberg-Institut)
D-80805 München (Germany)

H. Genz, H.-D. Gräf, P. Hoffmann-Stascheck, U. Nething, A. Richter

Institut für Kernphysik
Technische Hochschule Darmstadt
D-64289 Darmstadt (Germany)

W.-R. Dix, G. Illing, M. Lohmann, B. Reime, L. Schildwächter

HASYLAB at Deutsches Elektronen-Synchrotron DESY
D-22603 Hamburg (Germany)

80805 München · Föhringer Ring 6

X-ray Polarimetry using the Photoeffect in a CCD Detector

G. Buschhorn, R. Kotthaus, W. Kufner, W. Rößl, M. Rzepka, K.H. Schmidt

Max-Planck-Institut für Physik (Werner-Heisenberg-Institut)
D-80805 München (Germany)

H. Genz, H.-D. Gräf, P. Hoffmann-Stascheck, U. Nething, A. Richter

Institut für Kernphysik
Technische Hochschule Darmstadt
D-64289 Darmstadt (Germany)

W.-R. Dix, G. Illing, M. Lohmann, B. Reime, L. Schildwächter

HASYLAB at Deutsches Elektronen-Synchrotron DESY
D-22603 Hamburg (Germany)

Abstract

A new method of X-ray polarimetry based on the photoeffect in a finely segmented MOS charge coupled device (CCD) has been applied to monochromatic synchrotron radiation at HASYLAB at DESY and to planar channeling radiation at the superconducting electron linac S-DALINAC at Darmstadt. For the smallest pixel dimensions available today (6.8x6.8 μm^2) an analyzing power of 10% is observed at an energy of 33 keV. In addition to events from photoeffect in the thin depleted front layer of the CCD also diffusion spread events from much more abundant conversions deeper inside the chip were utilized for polarization analysis.

Submitted to *Nuclear Instruments and Methods in Physics Research A*

I. Introduction

With the advent of strong sources of polarized X-rays, like synchrotron and channeling radiation, polarization analysis is becoming an important experimental task. For example, the use of the polarization dependence of magnetic X-ray diffraction provides a natural method to analyse magnetism and phase transitions in solid states by X-ray scattering /1,2/. In addition to polarimetry of laboratory X-ray sources polarization analysis of X-rays from astronomical objects is extremely important for a better understanding of emission mechanisms, magnetic fields and source geometries /3/.

Polarimeters are based upon photon interactions which depend in a known way on the photon polarization. Established techniques at X-ray energies from a few to several hundred keV are large angle Compton scattering off quasifree electrons in amorphous targets /4,5/, Rayleigh scattering by bound electrons /6/ or 90° Bragg reflection /7/, whereas at energies in the multi-MeV range electron positron pair production in the Coulomb field of nuclei and, very recently, also of electrons /8/ have been utilized.

The scattering techniques have the advantage of a generally high analyzing power but suffer from not being compatible with simultaneous spectroscopy and imaging in which the incident photon is absorbed in the photoelectric effect.

Fraser /9/ first suggested to exploit the photoeffect also for the analysis of linear polarization by measuring the photoelectron angular distribution which is correlated with the photon beam polarization. With the availability of finely segmented charge coupled devices (CCDs) with pixel dimensions around or even below 10 μm it now appears feasible to measure very short electron tracks down to a few μm in Silicon. Recently, a small polarization effect was observed by Tsunemi et al. /10/, who analyzed synchrotron radiation between 15 and 37 keV using a CCD chip with 12 μm square pixels.

In the present study we have utilized a commercial optical CCD camera /11/ with substantially smaller pixels (6.8x6.8 μm^2) to measure the linear polarization of 33 keV synchrotron radiation and of planar channeling radiation in the range between 10 and 50 keV generated by 32 MeV electrons in a Beryllium crystal. The experiments were carried out at HASYLAB at DESY and at the superconducting electron linac S-DALINAC at the Institut für Kernphysik at the Technische Hochschule Darmstadt. The study evolved from our experiments on polarization of channeling radiation employing 90° Compton scattering /4,12/.

II. Method, apparatus and analysis procedures

II.1. Experimental method

The photoeffect can be exploited for polarization analysis of X-rays by measuring the direction of the emitted photoelectron (see fig.1). The angular distribution is given by

$$d\sigma_{ph}/d\Omega \sim (\mathbf{E} \cdot \mathbf{p_e})^2$$

where $\mathbf{E}$ is the electric field vector and $\mathbf{p_e}$ the photoelectron momentum. Thus, the photoelectron will be ejected preferentially perpendicular to the photon direction (i.e. in general in the detector plane) and along the $\mathbf{E}$ field vector. In order to measure the electron direction its ionization track in the detector medium has to be reconstructed. A Silicon pixel detector will allow to measure directional effects if the extension of the primary charge distribution is at least comparable to the pixel size. For Si and electrons of tens of keV the following empirical range energy relation holds /13/:

$$R(\mu m) = [E(keV)/10]^{1.75}.$$

Thus, a 10 keV electron will have a range of 1 µm only. Present Si technology will thus limit photoeffect polarimetry to energies above about 10 keV. The upper end of the range is given by the strong energy dependence of the photoeffect ($\sigma_{ph} \sim E^{-3.5}$) leading to detection efficiencies below 10^{-3} for typical Si MOS-CCDs with depletion thicknesses of a few µm. Ionization measurement using small size pixels is of no problem in the energy range of interest. A 30 keV photon produces a free charge of 8300 e^- well below the pixel saturation charge of modern CCDs (see table 1).

II.2. CCD Detector

The most important consideration in the choice of a detector for photoeffect polarimetry concerns the relation of pixel size to electron track length. Therefore, we have chosen a commercial optical CCD camera /11/ with the smallest presently available pixels (6.8x6.8 μm^2). The only modification necessary for our application was to remove a 750 µm thick cover glass protecting the CCD chip. Specifications relevant for X-ray detection are listed in table 1. The small pixel size of 6.8 µm is possible by choice of the 2 phase (rather than the more conventional 3 phase) shift technique requiring 2 instead of 3 electrodes per pixel. Implanted channel stops of 1.2 µm width between adjacent columns of pixels lead to a slight xy-asymmetry which may in part be responsible for an observed detector asymmetry (see section III). The very low dark current (< 10 pA/cm^2) at room temperature is achieved by operating the camera with all vertical clocks held at negative voltage except during charge transfer in order to pin the Si-SiO_2 interface potential to the substrate potential. When the

CCD is biased in this way holes accumulate near the interface where they recombine with electrons thermally generated via mid-gap interface states and thus reduce the dark current significantly /14/. The noise specifications were confirmed by taking dark pictures. Fig. 2 shows the noise distribution of all 1.3×10^6 pixels accumulated over 100 pictures (1.3×10^8 entries). The rms width of σ = 0.72 ADC channels corresponds to an energy equivalent of 150 eV. Throughout the analysis we selected significant pixels by a cut 4 channels (= 800 eV) above the noise peak. We chose such a high noise cut in order to reduce as much as possible the amount of data to be stored.

The CCD chip has an active (depleted) layer of a few µm thickness only which is followed by a field free layer and the Si substrate of total thickness of about 300 µm (see fig.1). Unlike visible light which interacts in the active front layer only, keV X-rays with absorption lengths of the order of mm will convert everywhere in the chip. Whereas the charge from X-rays absorbed within the depletion layer is swept by the strong electric field into the nearest potential well, charge created in the field free material beneath the depletion zone will spread out by diffusion and electrostatic repulsion before entering the depletion layer. Partial recombination and incomplete charge collection will cause these deep conversions to be detected with less than their full energy. Thus the photoeffect in the passive detector material below the active front layer will result in spread events with energy deficits. Charge diffusion effects have been studied extensively in the literature, both by simulation /15,16/ and experiment /16,17/. In our studies it turned out, that deep conversions do not confuse the energy spectra significantly (see paragraph II.4) and moreover, a large fraction of such events could be utilized for polarization analysis (see section III)

II.3. Data acquisition

Fig.3 shows schematically the data acquisition system. A camera control unit (CCU) provides the CCD clock (10 MHz) and synchronization signals to control the mode of operation of the camera. Since polarization analysis does not require to localize events on the CCD chip we chose to illuminate the CCD continuously during an exposure/readout cycle of 155 ms (10 ms exposure followed by a 145 ms readout period). This mode maximizes the duty cycle at the expense of giving up the spatial information in the charge shift direction (camera y-coordinate). Charge packets from the CCD output node are transferred at the shift frequency of 10 MHz to an 8 bit ADC housed inside the CCU. The digitized information is processed by a commercial frame grabber UPX 1000 /18/. The frame grabber is used to filter significant pixels by offset subtraction and energy discrimination in real time (i.e. within 100 ns) using appropriately programmed look up tables (input LUT). The UPX 1000 output (address and charge of each pixel) is transferred at 10 MHz to a graphics board UDC 2600 consisting of an

8 bit deep 2 Mbyte memory which is used to store one frame of 1280x1024 pixels. The UDC also serves as a monitor interface to display frames processed through output LUTs. The UDC 2600 memory is mapped via the 16 bit ISA bus of the host PC into the PC memory.
In order to minimize the amount of data written onto disk a fast online pattern recognition is done by identifying clusters (events) of contiguous significant pixels. Only significant pixels are kept for further offline analysis. Also, for the online control of the experiment it was important to have cluster information available, for instance, to display energy spectra and to monitor the xy-asymmetry of 2-pixel event rates. The online analysis causes deadtime which is to be minimized by optimizing the number of events per frame. For the measurements at HASYLAB (E = 33.17 keV) fig. 4 shows the rate at which events were taken as a function of the number of events per frame. The maximum data rate is around 80 events per sec. For the channeling radiation studies at S-DALINAC the event rate was raised to 200 Hz.

II.4. Laboratory tests with unpolarized X-rays

The CCD response to X-rays in the energy range between 5.9 and 31 keV was studied with X-ray fluorescence sources. Energy spectra of 1-pixel events selected by an energy cut of 800 eV per pixel are shown in fig. 5. At low energies (figs. 5 a-c) symmetrical photopeaks indicate charge containment within one pixel for the threshold given. At higher energies (figs. 5 d,e) the photopeaks develop a low energy tail and the continuum below the peaks increases due to incomplete charge collection by single pixels. The high threshold of 800 eV is far from optimal for precise energy measurement. The measured line widths of the low energy photopeaks (figs. 5 a-c) of about 350 eV (rms) are more than a factor of two larger than expected from electronics noise only (see paragraph II.2) and can be explained by a systematic contribution due to the charge transfer inefficiency (CTI < $3x10^{-5}$, see table 1) and by fluctuations of charge deposited in neighbouring pixels which is lost due to the high threshold. The optimization of selection procedures for energy spectroscopy will be subject of a forthcoming publication.
The pixel multiplicity of charge clusters was studied as a function of energy. Fig. 6 shows the most probable cluster size in number of contiguous pixels. Below 10 keV single pixel events are dominating whereas with increasing energy the clusters grow in size reaching most probable values of more than 10 pixels at 30 keV. Energy spectra of clusters (fig. 7) show that with increasing cluster size, i.e. for increasingly deeper conversions, the position of the photopeak shifts downwards as expected. This shift is plotted in fig. 8 for E = 22.2 keV (Ag K_{α} line) and E = 33.17 keV (monochromatic synchrotron radiation, see paragraph II.5). Photopeaks measured with multipixel clusters (fig. 7) are substantially broader (1.5 to 2.0 keV) than single pixel peaks (fig. 5) primarily due to threshold effects and (to a lesser extent)

increased noise contributions. The energy calibration extracted from photopeak positions is shown in fig. 9 for several multiplicity classes. In all classes we observe an approximate linear behaviour.

II.5. Synchrotron radiation test beam

Polarization measurements were done at the wiggler beam W2 HARWI /19/ of HASYLAB at DESY. A monochromator consisting of two bent Si crystals in Laue geometry filters two monochromatic beams of 33.17± 0.15 keV *) out of the white spectrum. For our purposes the energy spectrum can be considered as monochromatic. Fig. 10 gives the spectrum measured with the CCD when all cluster sizes are added. Being the superposition of slightly shifted lines (see fig. 8) the width of the photopeak is broad (4 keV fwhm) but still stands out clearly such that cuts can be made to isolate photoeffect events. In fig. 11 the measured beam profiles are plotted. In order to measure both the horizontal (squares) and vertical (circles) profiles the camera had to be rotated about the beam axis by 90° since, as discussed in paragraph II.3, the continuous mode of exposure allows us to measure the camera x-coordinate only. The beams are about 5 mm wide, 0.5 mm high and 2 mm apart vertically. The beam is linearly polarized in the horizontal plane to P = 83.6% /20/.
The beam flux (up to 10^{11} photons per s and mm^2) had to be reduced by about 6 orders of magnitude to achieve tolerable rates at the CCD. In order to minimize beam hardening (enhancement of the third harmonic at 99.5 keV) we used a graphite absorber of 28 cm to moderate the photon flux.

*) Normally, this beam line is used for digital subtraction angiography /19/ which requires a dichromatic double beam.

II.6. Channeling radiation

A polarized X-ray beam of channeling radiation (CR) was produced at the superconducting electron linac S-DALINAC /21/ by directing a low divergence electron beam of 32 MeV onto a 500 µm thick Be monocrystal cut in the (11.0) direction and mounted on a two axes goniometer /12/. Energy spectra of CR produced at the (00.1) and (11.0) planes measured with a Ge detector are shown in fig. 12 together with the respective backgrounds of bremsstrahlung recorded with the crystal in random orientation. To minimize the radiation

dose accumulated by the CCD we suppressed the low energy part of the spectra below the channeling spikes by a 2 mm thick Al absorber. Planar CR is 100% linear polarized perpendicular to the lattice plane /4,12/. Thus, from the measured energy spectra composed of CR and unpolarized bremsstrahlung the degree of beam polarization can be calculated. It equals the fractional CR yield. Table 2 compares the results obtained from spectra measured with the Ge detector and the CCD camera. Both measurements agree within errors which are dominated by uncertainties in the relative normalization of CR and bremsstrahlung spectra. The (11.0) spectrum is less strongly polarized than the (00.1) spectrum due to the much weaker CR contribution (see fig. 12). The two orthogonal polarization planes are oriented nearly vertically for the (00.1) plane and horizontally for the (11.0) plane of the Be crystal.

II.7. Polarization analysis

For the polarization analysis the asymmetry

$$A = (N_x - N_y)/(N_x + N_y)$$

is determined, where N_x (N_y) are the numbers of events oriented along the x- (y-) axis of the CCD chip. For 2-pixel events the subdivision into x- and y-classes is obvious. 3-pixel events are treated the same way as 2-pixel events after omitting the lowest energy pixel. For larger clusters ($n_{pix} > 3$) an event axis analysis is performed in the xy-plane in analogy to the analysis of moments of inertia by minimizing the quantity

$$M = \sum E_i \cdot r_i^2 ,$$

with E_i being the energy deposition in pixel i and r_i the distance of pixel i to the event axis.

In order to study the same asymmetry A as for 2- and 3-pixel events, the larger events are assigned to the x- and y-classes by subdividing the angular distribution of the event axis in two 90°-bins symmetrical about the x- and y-directions, respectively.

The axis analysis works well for large clusters ($n_{pix} > 5$), whereas for medium size clusters ($n_{pix} = 4,5$) the discrete pixel structure is strongly reflected in the axis distribution (e.g. for the 4-pixel events a strong peak occurs around 45°) and leads to rather unstable x- or y-assignments.

III. Results of polarization measurements

III.1. Polarization of synchrotron radiation

Fig. 13 shows measurements of the asymmetry A separately for different event classes from 2 to 9 pixels per event. The data were taken with two different CCD orientations (0°: x = horizontal, 90°: x = vertical). If A were only due to beam polarization it should change sign when rotating the camera by 90°, i.e. interchanging the x- and y-coordinates. The data are clearly not symmetric with respect to 0, reflecting a nonvanishing detector asymmetry A_{CCD}. Both, the polarization asymmetry A_{POL} and A_{CCD} can be determined separately from the 0°- and 90°-measurements:

$$A_{POL} = (A(0°) - A(90°))/2$$
$$A_{CCD} = (A(0°) + A(90°))/2$$

The results are displayed in figs. 14 and 15. In addition, fig. 15 shows a direct measurement of A_{CCD} with unpolarized X-rays from a CsI fluorescence source ($28 < E < 31$ keV). Both measurements agree reasonably well with each other except for clusters of 4 and 5 pixels. As discussed above (see paragraph II.7), an asymmetry measurement based on such medium size clusters is problematic with our method of analysis. The negative values of A_{CCD} for 2- and 3-pixel events (both treated as 2-pixel events) may, at least in part, be caused by the 1.2 µm wide channel stops oriented in the y-direction and thus leading to a reduced detection efficiency for x-oriented 2-pixel events compared to y-oriented ones. A slight xy-asymmetry is also observed in the 2-pixel energy spectra: The spectrum of x-oriented pixel pairs is slightly shifted downwards compared to the one for y-oriented pairs. For the small positive values of A_{CCD} for large clusters ($n_{pix} > 5$) from deep conversions we do not have a plausible explanation. As demonstrated by our results on A_{POL} in fig. 14, we definitely observe beam polarization for all cluster sizes. The effect is largest for 2-pixel events ($A_{POL} = 7.6\%$) and somewhat smaller for large (i.e. deep) events. Again, 4- and 5-pixel events behave erratic due to our axis analysis which is inappropriate for such small clusters. We point out that the large clusters from conversions deep inside the CCD chip are quite useful for polarization analysis inspite of charge diffusion and losses. In fact, the significance of A_{POL} is highest for large events, which are much more abundant than 2-pixel events making up only 0.3% of the whole event sample. From the measured A_{POL} and the calculated beam polarization ($P = 83.6\%$) /20/ we deduce an analyzing power $a = A_{POL}/P$ of about 10% for 2-pixel events and somewhat less for larger events.

III.2. Polarization of channeling radiation

Polarization of planar CR from Be was studied by measuring complete azimuthal angular distributions of A. The results for 2-pixel events are shown in fig. 16 for the (00.1) and (11.0) planes. The functional form

$$A = A_{CCD} + A_{POL} \cdot \cos 2(\varphi - \phi_{POL})$$

was fitted to the data, where A_{CCD} and A_{POL} are as defined in paragraph III.1, φ is the CCD azimuthal angle measured between the camera x-axis and the horizontal direction, ϕ_{POL} is the azimuthal angle of the polarization plane. The fit results are summarized in table 3. As for synchrotron radiation, we observe a definite polarization effect and in addition a nonvanishing camera asymmetry A_{CCD} consistent with our HASYLAB measurements at 33.17 keV and laboratory studies with unpolarized sources (see fig. 15). The measured A_{CCD} is further confirmed by asymmetry measurements with unpolarized bremsstrahlung (see fig. 16a). The φ-distributions of A clearly show the orthogonal orientations of the polarization planes for the two channeling planes (00.1) and (11.0) of Be. From crystal alignment based on measurements of channeling radiation yields maximum asymmetry is expected for ϕ_{POL} = 85.7° for the (00.1) plane and -4.3° for the (11.0) plane. The fits for ϕ_{POL} of our measurements (see table III) are in fair agreement with these expectations, considering the fact that the phase ϕ_{POL} is very sensitive to small variations of the CR spectra and their effective polarization. We have observed such variations by periodically taking energy spectra with the Ge detector during the course of the CCD measurements. In view of such somewhat incompletely controlled systematics we have chosen not to assign quantitative errors to our fit results in table 3. A comparison of A_{POL} measured for the two channeling planes clearly reflects the different degrees of polarization extracted from the measured mixtures of CR and bremsstrahlung for the two planes (see table 2). The average analyzing power $a = A_{POL} / P$ in the energy range from 12 to 60 keV is around 5 to 6% (see last column in table 3). This result is strongly dominated by the low energy data within this interval.

A more complete analysis of the orientation of polarization planes was performed by fitting the azimuthal angular distributions of cluster orientations of events with more than three pixels. For each azimuth φ the angle α between this direction and the polarization plane was determined by finding the direction of maximum asymmetry. The result for 6-pixel events is given in fig. 17 together with linear fits ($\alpha = a \cdot \varphi + \phi_{POL}$) yielding the azimuths ϕ_{POL} = 86.7° and ϕ_{POL} = -13.2° for the (00.1) and (11.0) planes, respectively, in reasonable agreement with expectations from crystal alignment. Interesting to note is the modulation of experimental angles α with respect to straight line fits which reflects the CCD asymmetry A_{CCD} reinforcing or weakening the polarization asymmetry A_{POL} depending on the camera angle φ.

IV. Discussion and conclusions

Fraser's proposal /9/ to utilize the photoeffect for X-ray polarimetry has been explored experimentally in the energy range from 10 keV to about 50 keV using a commercial CCD camera with the smallest pixels (6.8x6.8 μm^2) available today.

We have measured the linear polarization of monochromatic synchrotron radiation of 33.17 keV and of planar channeling radiation produced by 32 MeV electrons in a Be monocrystal. Compared to previous measurements /10/ on synchrotron radiation using a CCD with 12 µm pixels the polarization asymmetry measured in our studies is substantially increased by the small pixel size of our CCD chip. Recent simulations by Holland et al. /22/ of our synchrotron radiation measurements are in very good agreement with our result (fig. 18). In order to compare to the asymmetry calculations of /22/, which were done for a linear polarization of 84% corresponding to the experimental conditions at HASYLAB, our asymmetry measurements of channeling radiation with a smaller effective linear polarization (see table 2) had to be scaled by the ratio of polarizations. A more detailed study of the energy dependence of the analyzing power as was possible in these experiments requires monochromatic X-rays and will be done in the near future.

We have shown that in addition to 2-pixel events primarily due to photoeffect in the depleted front layer of the CCD the much more abundant multipixel events (> 3 pixels/event) from photon conversions deeper inside the CCD chip can be utilized for polarization analysis as well. Even though degraded by diffusion and incomplete charge collection these deep events show a clear polarization asymmetry with an analyzing power only slightly lower than for 2-pixel events.

Inherent detector asymmetries were observed which depend on cluster size, X-ray energy, energy cutoff and possibly further parameters. Although these CCD asymmetries, having to do with the chip architecture, can be determined by measurements with unpolarized X-rays or by measuring angular distributions of asymmetries they deserve further study both by systematic measurements and simulations.

In order to fully exploit the potential of photoeffect polarimetry attempts to enhance the analyzing power of presently 10% should be made by applying more refined analysis procedures, e.g. selection of special event classes with high directional sensitivity and a more detailed analysis of the charge deposition with reduced thresholds.

Most important for further development of the method would be advances in small pixel CCD technology. Substantially deeper depletion layers would enhance the detection efficiency and thereby extend the useful range of energy. Efforts in this direction are being made /22/. Deeply depleted pn-CCDs /23/ based on the principle of the Si driftchamber /24/ are presently being fabricated for satellite X-ray missions /25/. These devices are very promising

for spectroscopy and imaging of X-rays with high detection efficiencies but are presently limited to linear pixel dimensions of order 100 μm which is too large for photoeffect polarimetry in the X-ray regime of tens of keV.

To summarize, a new type of X-ray polarimeter based on the photoeffect in a finely segmented optical CCD has been studied in detail with a view to the development of a universal X-ray detector for simultaneous polarization, energy and position measurement.

Acknowledgements

This work was supported by the German Federal Minister for Research and Technology (BMFT) under contract Nr. 06DA641I. The authors wish to thank the S-DALINAC group at Darmstadt, in particular E. Spamer, and the technical staff of the Max-Planck-Institut für Physik, in particular W. Erbe, for the operation of the accelerator and for technical support. We also like to thank G. W. Fraser, A. Holland, A. Short and L. Strüder for discussions and useful comments and J. Pflüger for calculating the synchrotron beam polarization. The MPI authors gratefully acknowledge the hospitality extended to them at HASYLAB and at the Institut für Kernphysik, TH Darmstadt.

References

1. M. Blume and D. Gibbs, Phys. Rev. **B37** (1988) 1779
2. D. Gibbs, Syn. Rad. News **5** (1992) 18
3. G.W. Fraser, " X-ray detectors in astronomy", monograph, Cambridge Univ. Press (1989)
4. E. Diedrich, G. Buschhorn, W. Kufner, M. Rzepka, H. Genz, H.-D. Gräf, P. Hoffmann-Stascheck and A. Richter, Phys. Lett. **A178** (1993) 331
5. F. Smend, D. Schaupp, H. Czerwinski, A.H. Millhouse and H. Schenk-Strauss, Nucl. Instr. and Meth. **A241** (1985) 290
6. L. Kissel, R.H. Pratt and S.C. Ray, Phys. Rev. **A22** (1980) 1970
7. Th. Brückel, V. Rilling, W. Prandl, M. Lippert and J.R. Schneider, "A New Polarization Analyzer", HASYLAB Annual Report (1992) 631
8. Y. Iwata, I. Endo, M. Tobiyama, T. Kobayashi, A. Isobe, T. Nishizuru, K. Yoshida, M. Muto, T. Emura, K. Nagata, Y. Nagata, K. Baba and M. Asai, Nucl. Instr. and Meth. **A336** (1993) 146
9. G.W. Fraser, SPIE Vol.**1140** X-Ray Instrumentation (1989) 50
10. H. Tsunemi, K. Hayashida, K. Tamura, S. Nomoto, M. Wada, A. Hirano and E Miyata, Nucl. Instr. and Meth. **A321** (1992) 629
11. Eastman Kodak MEGAPLUS Camera Model 1.4 using CCD chip KAF-1400
12. M. Rzepka, G. Buschhorn, E. Diedrich, R. Kotthaus, W. Kufner, W. Rößl, K.H Schmidt, H. Genz, H.-D. Gräf, P. Hoffmann-Stascheck and A. Richter, Proc. **ICACS-15**, London, Ontario, Canada (1993)
13. J. Janesick, T. Elliott and G. Garmire, SPIE Vol.**597** X-Ray Instr. in Astron. (1985) 364
14. N.S. Saks, IEEE Trans. Electr. Dev. Lett. **EDL-1** (1980) 131
15. G.R. Hopkinson, Nucl. Instr. and Meth. **216** (1983) 423
16. N. Meidinger, Max-Planck-Inst. f. Extraterr. Phys. Report **225** (1991)
17. D.H. Lumb and G.R. Hopkinson, Nucl. Instr. and Meth. **216** (1983) 431
18. UNIVISION Model O-SDSL
19. W.-R. Dix, K. Engelke, W. Graeff, C. Hamm, J. Heuer, B. Kaempf, W. Kupper, M. Lohmann, B. Reime and R. Reumann, Nucl. Instr. and Meth **A314** (1992) 307
20. J. Pflüger (HASYLAB at DESY), private communication (1993)
21. J. Auerhammer, H. Genz, H.-D. Gräf, R. Hahn, P. Hoffmann-Stascheck, C. Lüttge, U. Nething, K. Rühl, A. Richter, T. Rietdorf, P. Schardt, E. Spamer, F. Thomas, O. Titze, J. Töpper and H. Weise, Nucl. Phys. **A553** (1993) 841c
22. A.D. Holland (Leicester Univ., X-Ray Astronomy Group), private communication (1993)
23. L. Strüder, P. Holl, G. Lutz and J. Kemmer, Nucl. Instr. and Meth. **A253** (1987) 386
    L. Strüder, Max-Planck-Inst. f. Physik Report **MPI-PAE/Exp.El. 208** (1989)
24. E. Gatti and P. Rehak, Nucl. Instr. and Meth. **A225** (1984) 608

25. L. Strüder, H. Bräuninger, M. Meier, P. Predehl, C. Reppin, M. Sterzik, J. Trümper, P. Cattaneo, D. Hauff, G. Lutz, K.F. Schuster, A. Schwarz, E. Kenziorra, A. Staubert, E. Gatti, A. Longoni, M. Sampietro, V. Radeka, P. Rehak, S. Rescia, P.F. Manfredi, W. Buttler, P. Holl, J. Kemmer, U. Prechtel and T. Ziemann, Nucl. Instr. and Meth. **A288** (1990) 227

H. Bräuninger, R. Danner, D. Hauff, P. Lechner, G. Lutz, N. Meidinger, E. Pinotti, C. Reppin, L. Strüder, J. Trümper, E. Kendziorra, J. Krämer, M. Mohan, R. Staubert, N. Findeis, P. Holl, J. Kemmer and C. von Zanthier, Nucl. Instr. and Meth. **A326** (1993) 129

Figure captions

Fig. 1: Principle of photoeffect polarimetry. The distribution of angles Θ between the electric field vector **E** and the photoelectron momentum $\mathbf{p_e}$ is the polarization analyser.

Fig. 2: CCD noise distribution measured with dark events. The rms width of $\sigma = 0.72$ channels corresponds to 150 eV.

Fig. 3: Schematics of data acquisition system (see text).

Fig. 4: Event rate as a function of the number of events per frame. The rate is determined by dead time introduced through online pattern recognition.

Fig. 5: Single pixel energy spectra measured with X-ray fluorescence sources: a) Mn, b) Cu, c) Ge, d) Mo, e) Ag (threshold: 800 eV/pixel)

Fig. 6: Most probable cluster size as a function of energy (threshold: 800 eV/pixel). 1 channel corresponds to 200 eV.

Fig. 7: Sum energy spectra of clusters produced by Ag K_{α} X-rays (E = 22.2 keV): a) 2-pixel clusters, b) 4-pixel clusters, c) 6-pixel clusters, d) 8-pixel clusters 1 channel corresponds to 200 eV.

Fig. 8: Measured energy sums for clusters of different size at photon energies of 22.2 keV (Ag K_{α}) and 33.17 keV (monochromatic synchrotron radiation).

Fig. 9: Energy calibration for clusters of 1, 2 and 3 pixels

Fig. 10: Energy spectrum measured for 33.17 keV synchrotron radiation. Clusters of all sizes are added. The bulge around channel 80 is interpreted as fluorescence of Ag inside the camera close to the CCD chip. 1 channel corresponds to 200 eV.

Fig. 11: Synchrotron radiation beam profile measured with two orthogonal camera orientations: 0° measurement: horizontal profile, 90° measurement: vertical profile. Pixel size is 6.8 µm.

Fig. 12: Channeling radiation spectra measured with a Ge detector for 32 MeV electrons together with bremsstrahlung backgrounds:
a) (00.1) plane of Be
b) (11.0) plane of Be
Low energy radiation is suppressed by 2 mm of Al.

Fig. 13: Asymmetry measurements for 33.17 keV synchrotron radiation as a function of cluster size. Data were taken with two different camera orientations (0° and 90°) to determine polarization and detector asymmetries separately (see text).

Fig. 14: Polarization asymmetry of 84% linear polarized synchrotron radiation of 33.17 keV as a function of cluster size.

Fig. 15: Detector asymmetry as a function of cluster size measured with 33.17 keV synchrotron radiation and with unpolarized X-rays from a CsI fluorescence source ($28 < E < 31$ keV)

Fig. 16: Azimuthal angular distribution of 2-pixel event asymmetry for planar Be channeling radiation in the energy interval of 12 to 60 keV:
a) (00.1) plane, b) (11.0) plane

Fig. 17: Azimuths α of polarization planes with respect to camera azimuths φ as a function of φ as determined from angular distributions of 6-pixel events for Be planes (00.1) and (11.0). Straight lines are linear fits $\alpha = a\,\varphi + \Phi_{POL}$. The modulation of the data points reflects the CCD asymmetry reinforcing or weakening the polarization asymmetry depending on the camera angle φ.

Fig. 18: Comparison of asymmetry measurements of 33.17 keV synchrotron radiation and planar channeling radiation with simulations done by Holland et al. /22/ for the conditions of our experiment.

Table 1

Parameters and specifications of CCD KAF-1400

Parameter	Specification
architecture	front illuminated, full frame
technology	MOS-BCCD, 2 phase, 2 level poly-Silicon
number of pixels	1340(H)x1037(V)
pixel size	6.8x6.8 μm^2
sensitive area	9x7 mm^2
sensitive fill factor	100%
pixel saturation signal	$4.5x10^4$ e^-
dark noise (T = 25°C)	25 e^-
dark current (T = 25°C)	< 10 pA cm^{-2}
dynamic range	60 dB
clock frequency	10 MHz
readout time	145 msec
charge transfer inefficiency	$< 3x10^{-5}$
output sensitivity	12 µV/electron

Table 2

Be Channeling radiation polarization as inferred from energy spectra

Detector	Plane	Energy Interval	Polarization
Ge	(00.1)	16 - 60 keV	70 ± 1 %
		16 - 37 keV	67 ± 1 %
CCD		12 - 60 keV	71 ± 2 %
		12 - 32 keV	72 ± 2 %
Ge	(11.0)	16 - 60 keV	31 ± 1 %
		16 - 40 keV	35 ± 1 %
CCD		12 - 60 keV	32 ± 2 %
		12 - 32 keV	33 ± 2 %

Table 3

Asymmetry results for planar channeling radiation off Be

Plane	Energy Interval	A_{POL}	Φ_{POL}	A_{CCD}	$a = A_{POL}/P$
(00.1)	12 - 60 keV	3.7 %	77.3°	-3.0 %	5.2 %
	12 - 32 keV	3.7 %	78.0°	-2.9 %	
	10 - 16 keV	4.2 %	83.4°	5.7 %	
	10 - 22 keV	3.3 %	75.0°	-4.3 %	
(11.0)	12 - 60 keV	2.0 %	-0.7°	-2.2 %	6.3 %

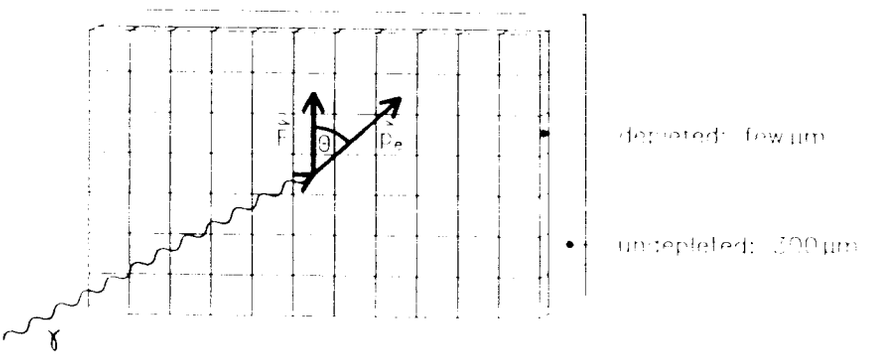
θ
depleted: few µm
undepleted: 300 µm
γ

Fig. 1

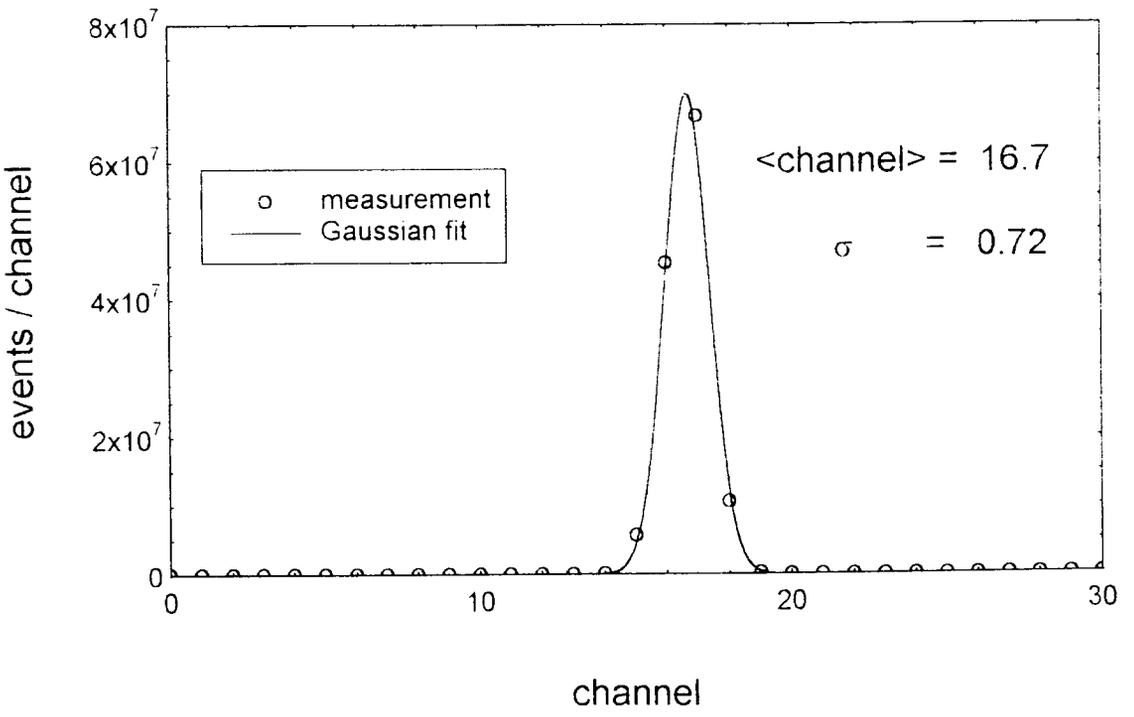
8x10^7
6x10^7
4x10^7
2x10^7
0
events / channel
measurement
Gaussian fit
<channel> = 16.7
σ = 0.72
0
10
20
30
channel

Fig. 2

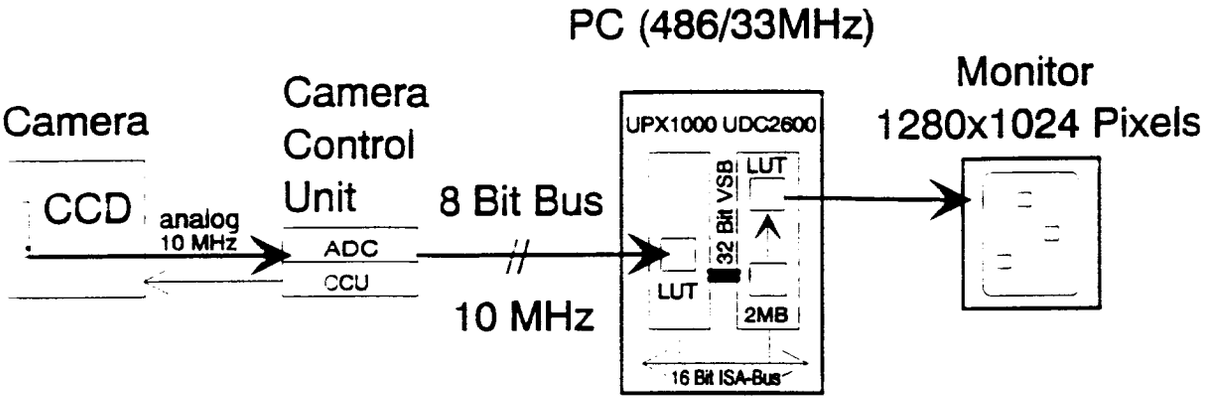
PC (486/33MHz)
Camera
CCD
analog
10 MHz
Camera
Control
Unit
ADC
CCU
8 Bit Bus
10 MHz
UPX1000 UDC2600
LUT
32 Bit VSB
LUT
2MB
16 Bit ISA-Bus
Monitor
1280x1024 Pixels

Fig. 3

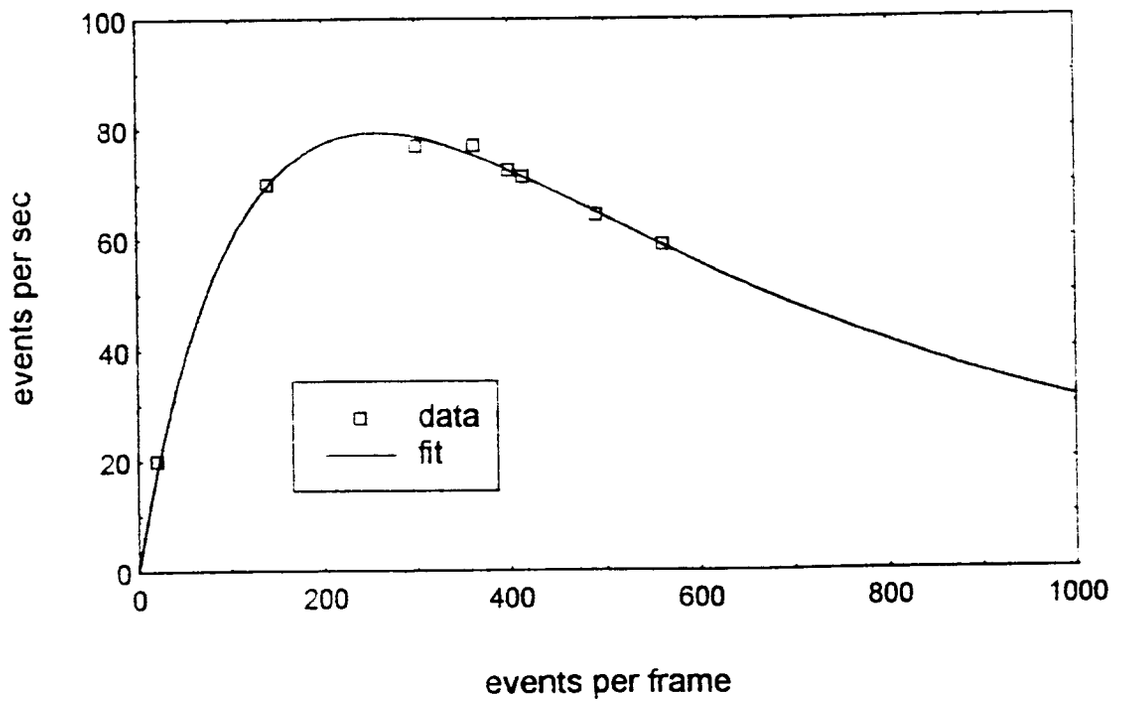
100
80
60
40
20
0
events per sec
data
fit
0
200
400
600
800
1000
events per frame

Fig. 4

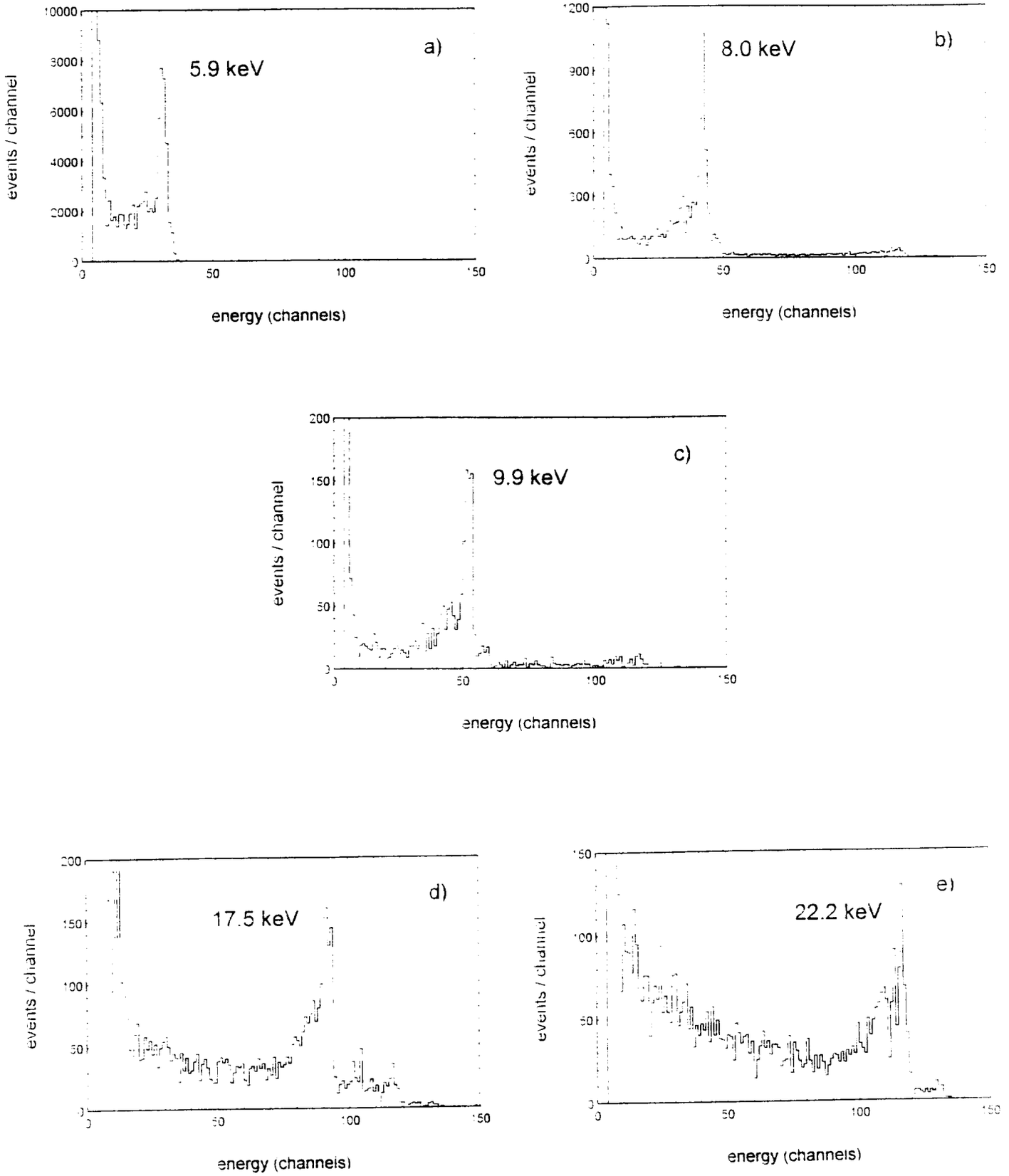
a)
5.9 keV
events / channel
energy (channels)
b)
8.0 keV
events / channel
energy (channels)
c)
9.9 keV
events / channel
energy (channels)
d)
17.5 keV
events / channel
energy (channels)
e)
22.2 keV
events / channel
energy (channels)

Fig. 5

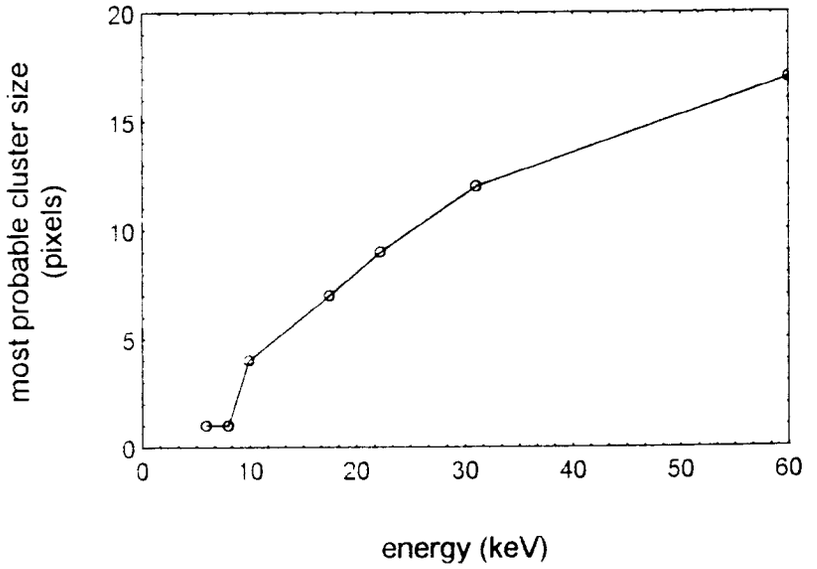
most probable cluster size (pixels)
energy (keV)
0
5
10
15
20
0
10
20
30
40
50
60

Fig. 6

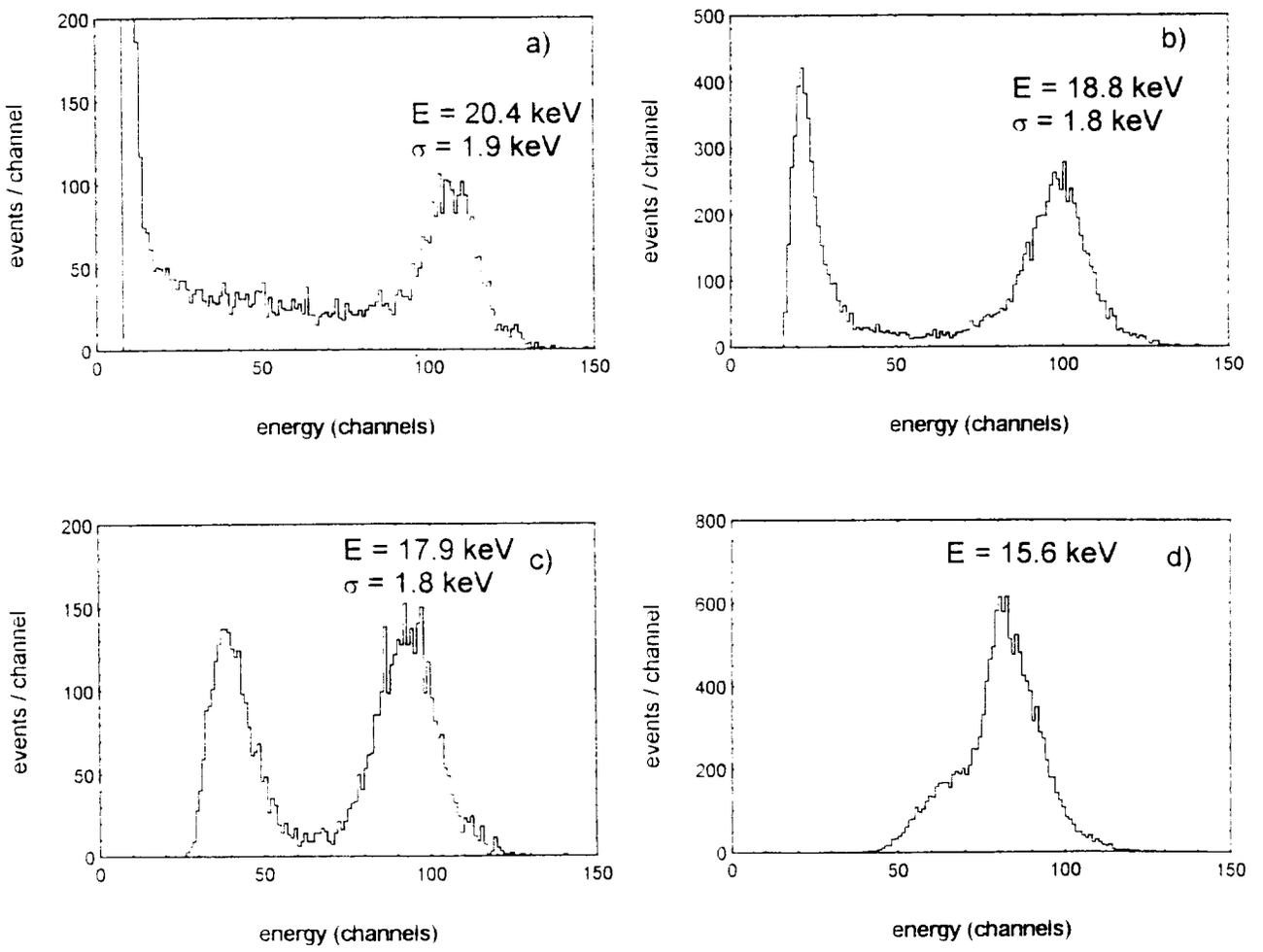
a)
E = 20.4 keV
σ = 1.9 keV
b)
E = 18.8 keV
σ = 1.8 keV
c)
E = 17.9 keV
σ = 1.8 keV
d)
E = 15.6 keV
events / channel
energy (channels)

Fig. 7

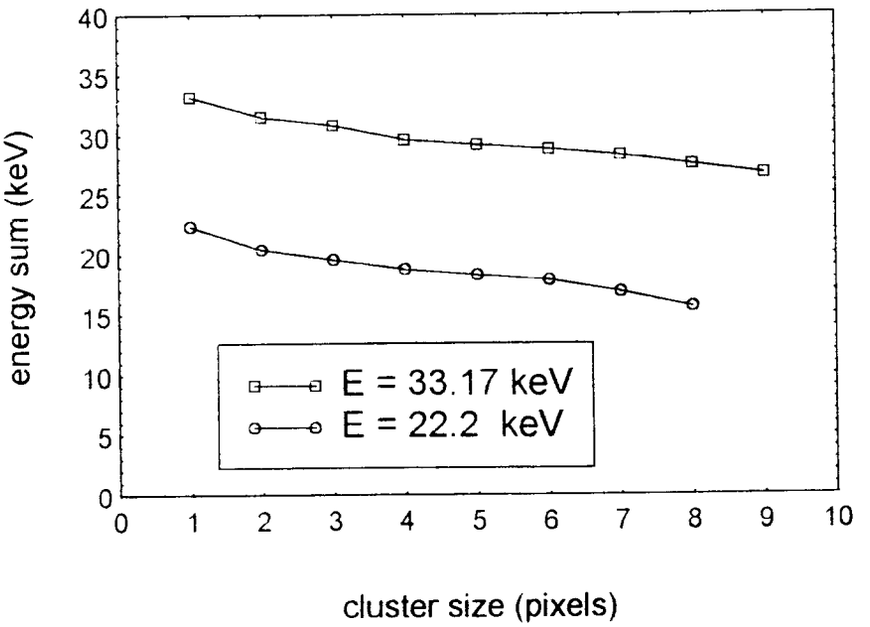
energy sum (keV)
cluster size (pixels)
E = 33.17 keV
E = 22.2 keV
0
5
10
15
20
25
30
35
40
0
1
2
3
4
5
6
7
8
9
10

Fig. 8

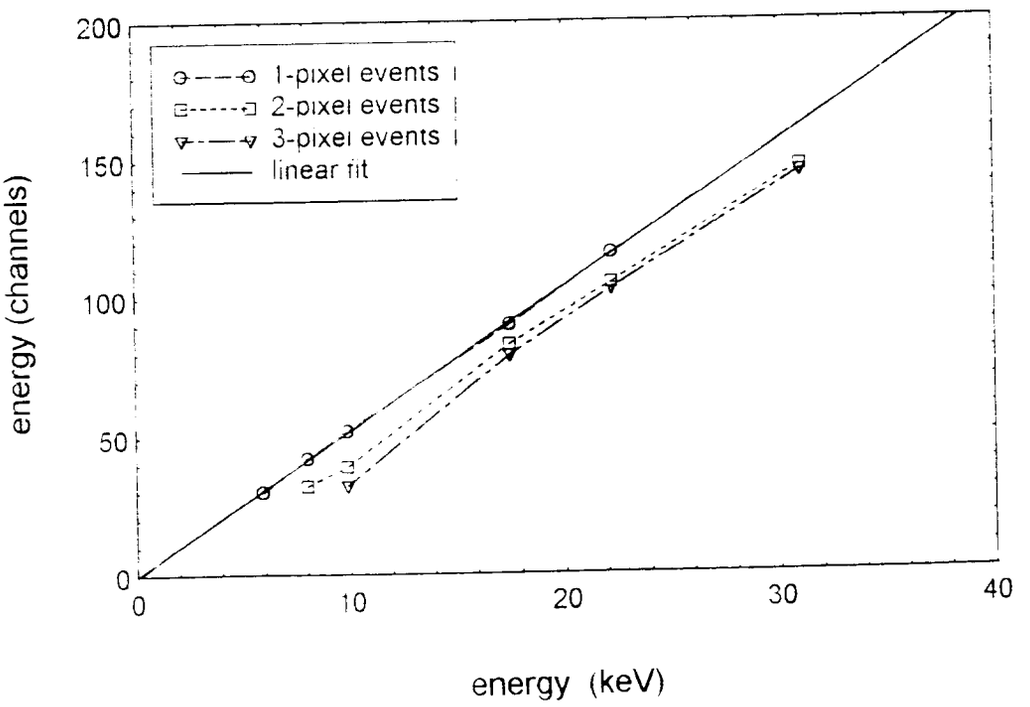
energy (channels)
energy (keV)
1-pixel events
2-pixel events
3-pixel events
linear fit
0
50
100
150
200
0
10
20
30
40

Fig. 9

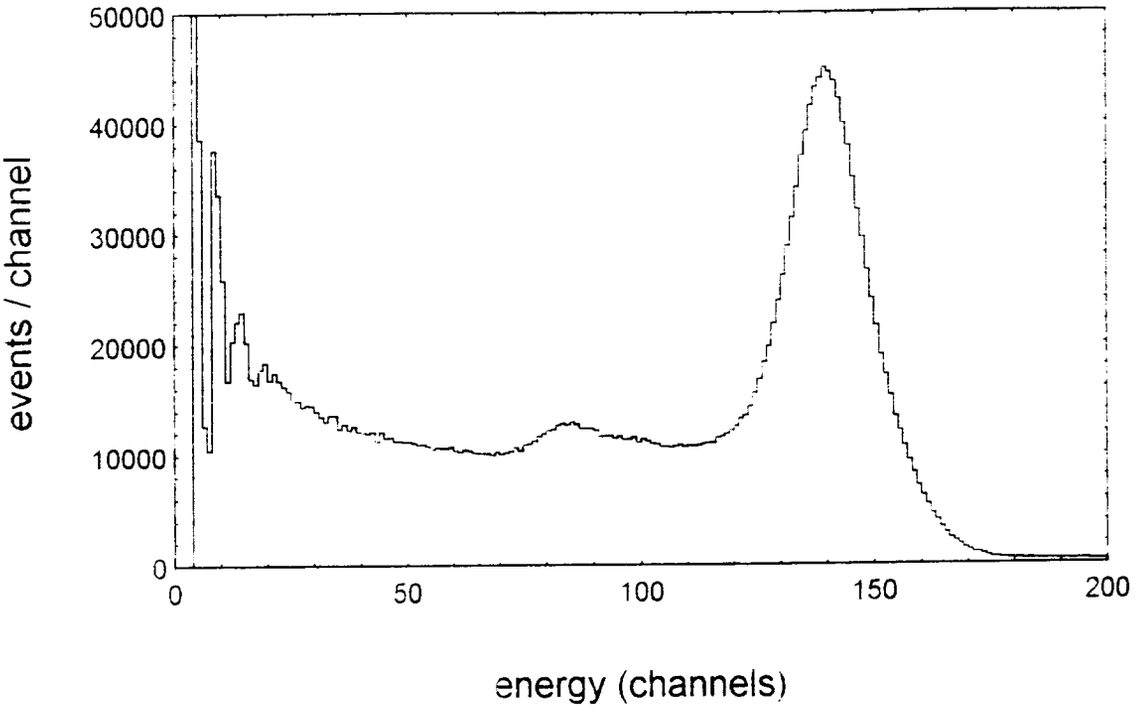
50000
40000
30000
20000
10000
0
events / channel
0
50
100
150
200
energy (channels)

Fig. 10

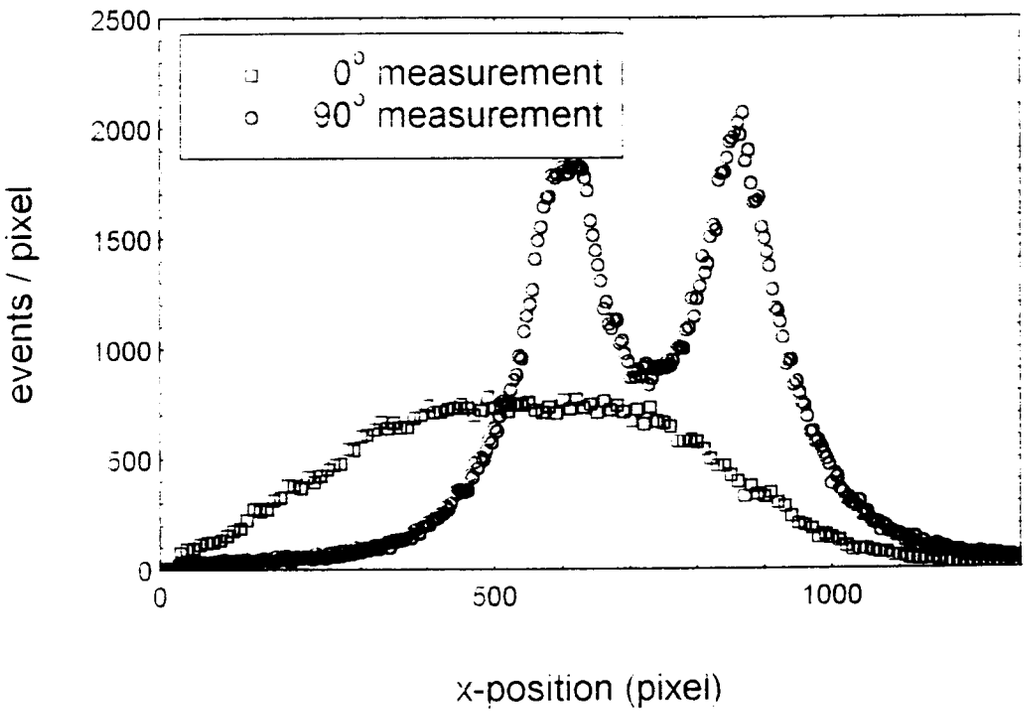
2500
2000
1500
1000
500
0
events / pixel
0° measurement
90° measurement
0
500
1000
x-position (pixel)

Fig. 11

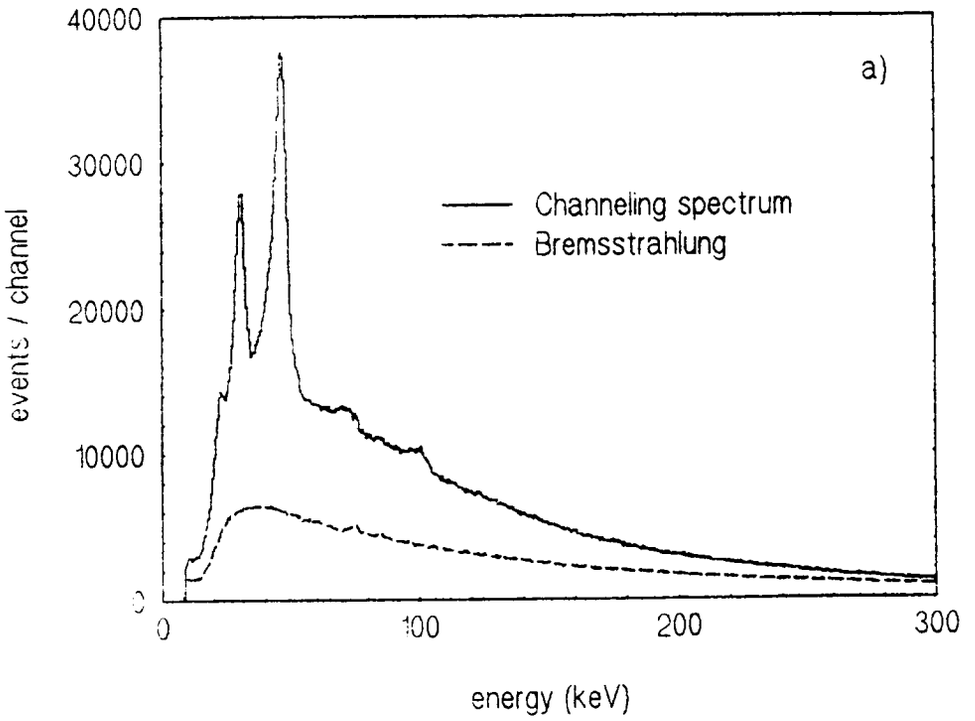
40000
30000
20000
10000
0
events / channel
a)
Channeling spectrum
Bremsstrahlung
0
100
200
300
energy (keV)

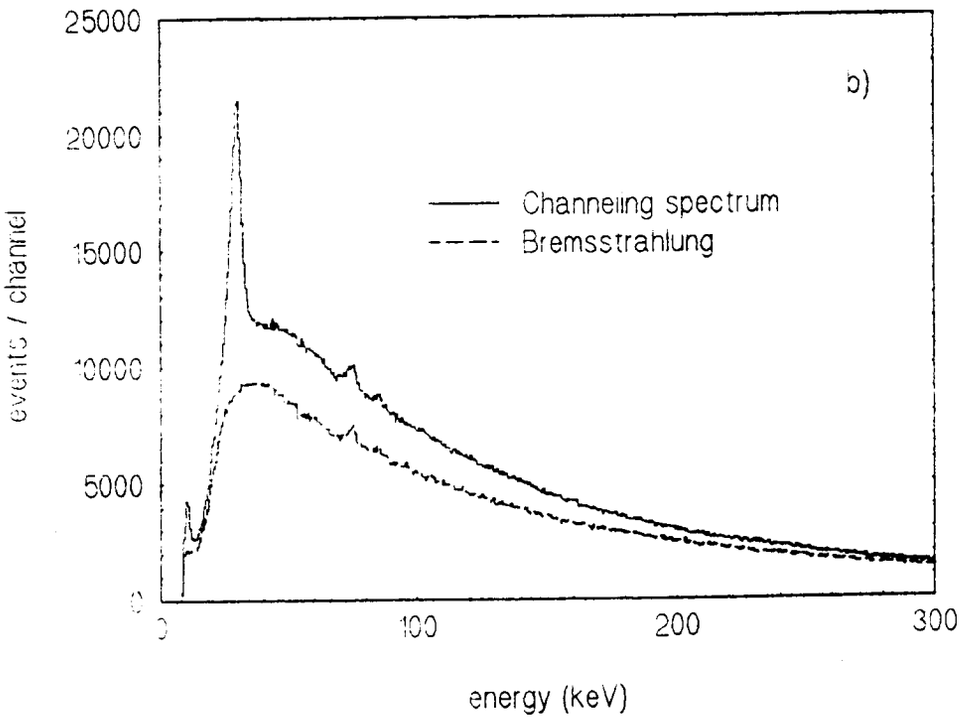
25000
20000
15000
10000
5000
0
events / channel
b)
Channeling spectrum
Bremsstrahlung
0
100
200
300
energy (keV)

Fig. 12

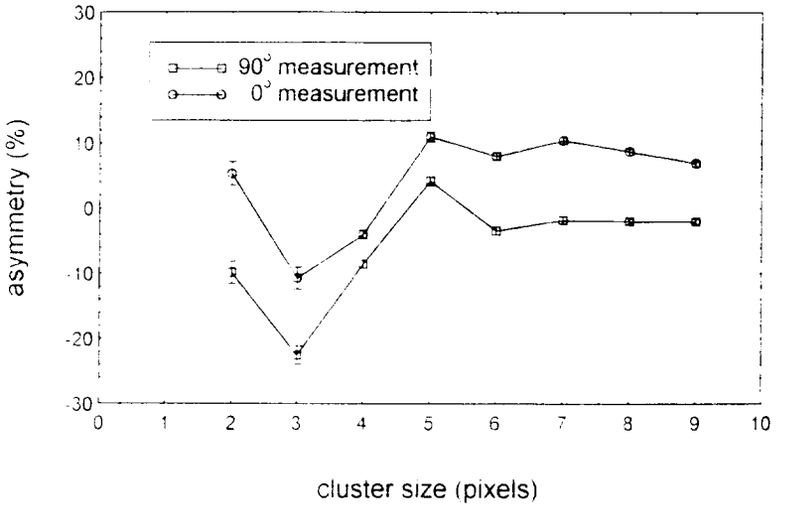

Fig. 13

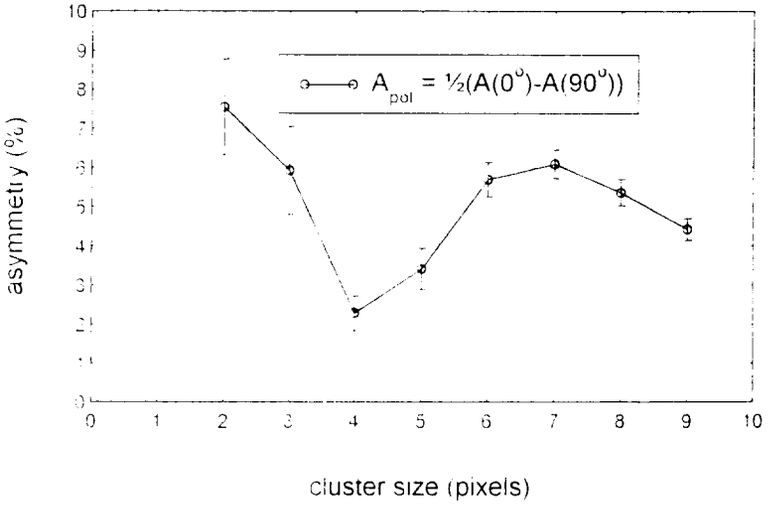

Fig. 14

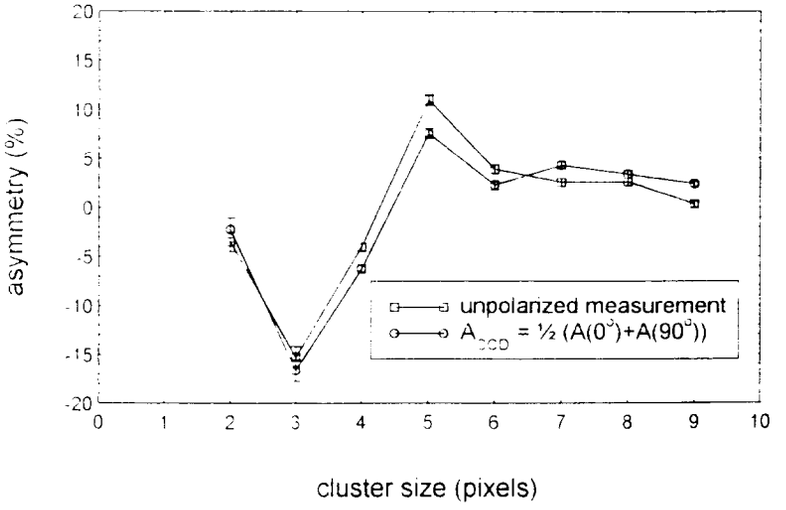

Fig. 15

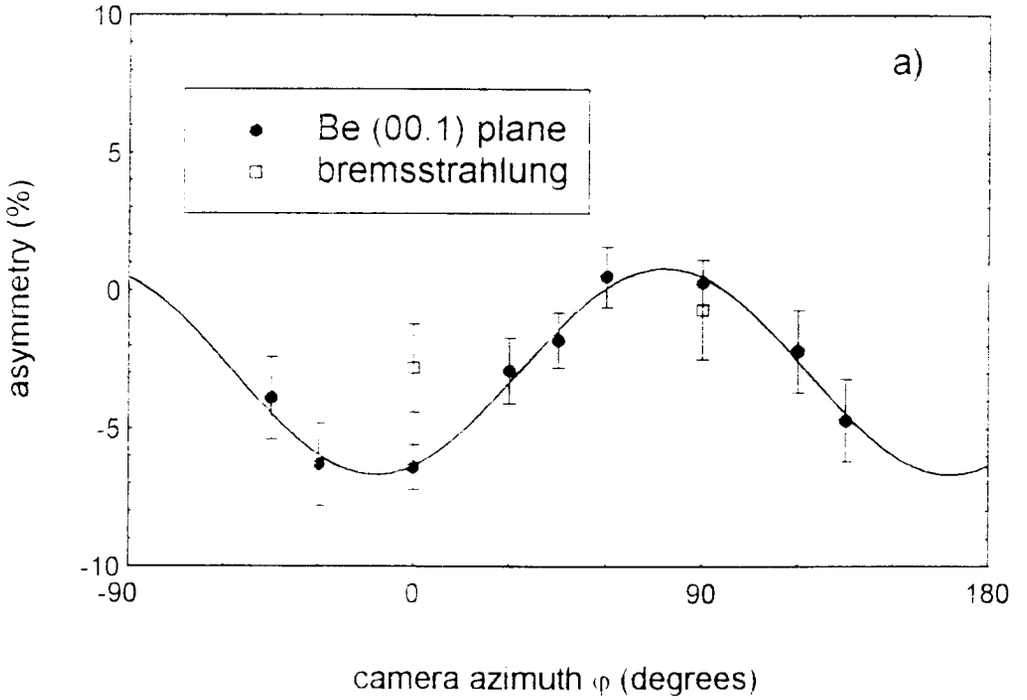
a)
Be (00.1) plane
bremsstrahlung
asymmetry (%)
10
5
0
-5
-10
-90
0
90
180
camera azimuth φ (degrees)

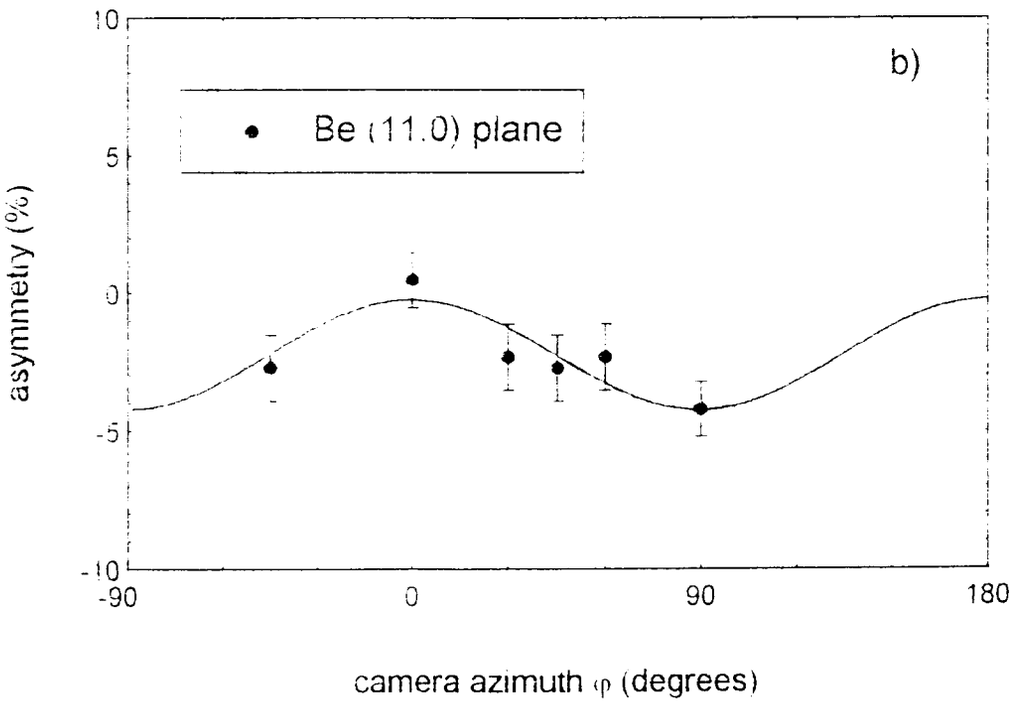
b)
Be (11.0) plane
asymmetry (%)
10
5
0
-5
-10
-90
0
90
180
camera azimuth φ (degrees)

Fig. 16

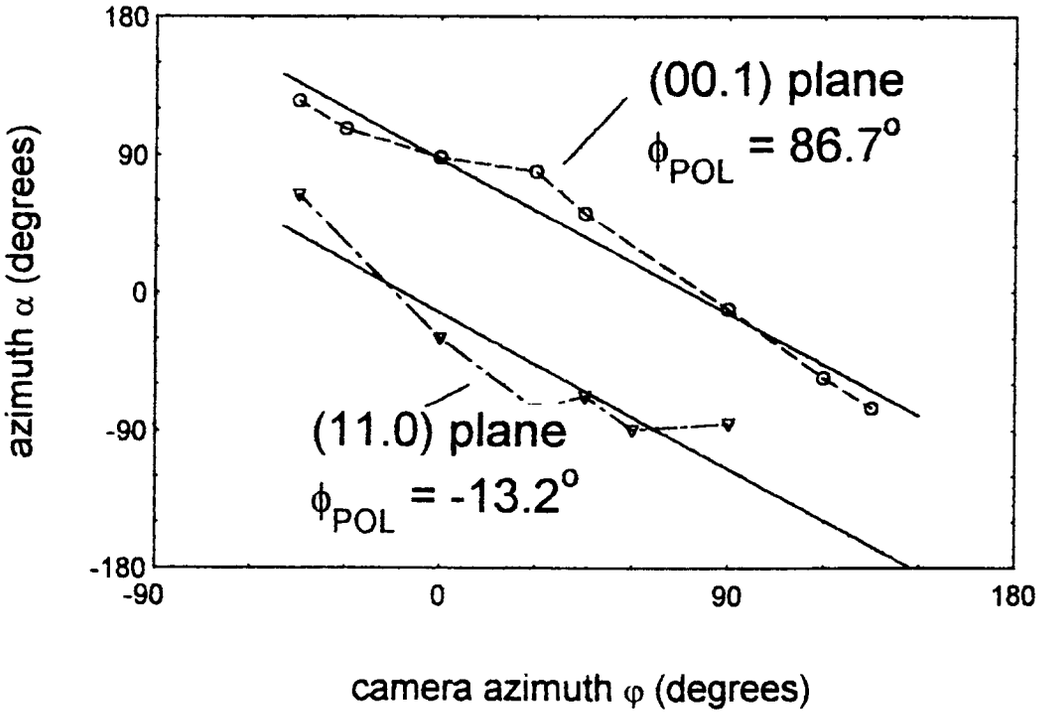
180
90
0
-90
-180
-90
0
90
180
azimuth α (degrees)
camera azimuth φ (degrees)
(00.1) plane
ϕ_{POL} = 86.7°
(11.0) plane
ϕ_{POL} = -13.2°

Fig. 17

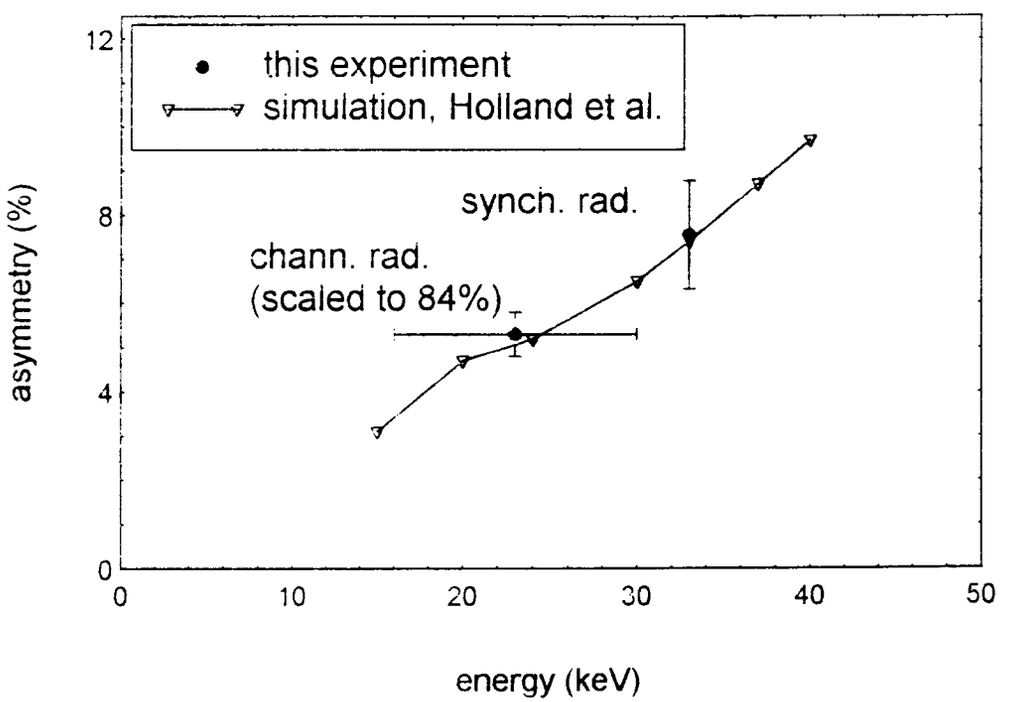
12
8
4
0
0
10
20
30
40
50
asymmetry (%)
energy (keV)
this experiment
simulation, Holland et al.
synch. rad.
chann. rad.
(scaled to 84%)

Fig. 18